PCCP

Accepted Manuscript

ROYAL SOCIETY OF CHEMISTRY

www.rsc.org/pccp

Multi-level quantum mechanics and molecular mechanics study of S_N2 reaction at nitrogen: $NH_2Cl + OH^-$ in aqueous solution

Jing Lv[†], *Jingxue Zhang*[‡], *Dunyou Wang*[*†]

[†] College of Physics and Electronics, Shandong Normal University, Jinan 250014, Shandong, China

[‡] School of Physics, Nankai University, Tianjin 300071, China

* Author to whom correspondence should be addressed. Email: dywang@sdnu.edu.cn

ABSTRACT

We employed a multi-level quantum mechanics and molecular mechanics approach to study the $NH_2Cl + OH^-$ in aqueous solution. The multi-level quantum method (including DFT method with both the B3LYP and M06-2X exchange-correlation functionals and CCSD(T) method, and both methods with the aug-cc-pVDZ basis set) was used to treat the quantum reaction region in different stages of the calculation in order to get an accurate potential of mean force. The obtained free energy activation barriers at DFT/MM level of theory yielded a big difference at 21.8 kcal/mol with the B3LYP functional and 27.4 kcal/mol with the M06-2X functional respectively. Nonetheless, the barrier heights become very close when shifted from DFT to CCSD(T): 22.4 kcal/mol and 22.9 kcal/mol under CCSD(T)(B3LYP)/MM and CCSD(T)(M06-2X)/MM levels of theory, respectively. The free reaction energy obtained with CCSD(T)(M06-2X)/MM shows excellent agreement with the one calculated using available gas-phase data. Aqueous solution plays a significant role in shaping the reaction profile. In total, the water solution contributes 13.3 kcal/mol and 14.6 kcal/mol to the free energy barrier heights under CCSD(T)(B3LYP)/MM and CCSD(T)(M06-2X)/MM respectively. The title reaction at nitrogen is a faster reaction than the corresponding reaction at carbon, $CH_3Cl + OH^-$.

Ⅰ. INTRODUCTION

Bimolecular nucleophilic substitution (S_N2) reactions hold an essential role in organic chemistry[1-3]. The S_N2 reaction at carbon (C) is probably the most intensively studied both theoretically[4-11] and experimentally[12-16], especially those reactions involving halogenated hydrocarbons since they are the major pollutants to surface/ground water and environment[17]. Comparatively, the S_N2 reactions at nitrogen (N) are rather less investigated. Therefore, it is necessary to study and understand the S_N2 reactions at nitrogen both in gas phase and solution phase.

Chloramines have been widely used as chemical disinfectants with monochloramine (NH_2Cl) being the most effective one. Presently many water treatment facilities use monochloramine to disinfect drinking water because NH_2Cl lasts longer in water pipes and produces fewer disinfection by-products[18]. In gas phase, Bühl and Schaefer[19] studied the transition state geometries and intrinsic barriers of S_N2 reactions at nitrogen at the *ab initio* DZP+/SCF level of theory, and found that the intrinsic barriers involving nitrogen are larger than those involving carbon. Xing et al.[20] investigated the correlation between energy and electron density representations of reactivity of S_N2 reactions at nitrogen with DFT/MPW1K/6-311++G(d,p) level of theory, which gives a barrier height of 15.4 kcal/mol for the title reaction $NH_2Cl + OH^-$. Yu et al.[21] studied the reaction mechanism of OH^- with NH_2Cl using *ab initio* molecular dynamics simulations and concluded that the typical back-side attack S_N2 reaction mechanism is the dominant reaction pathway in gas phase; they also calculated the barrier heights with

all-electron CCSD(T)/6-311++G(3df,2p) level of theory at 10.4 kcal/mol and with MP2(full)/6-31+G(d) at 11.4 kcal/mol respectively. In addition, an *ab initio* molecular orbital study at G2(+) level of theory by Glukhovtsev et al.[22] predicted that the barrier heights of the S_N2 reactions with $X^- + NH_2X$ (X=F, Cl, Br, I) are lower than the corresponding reactions with CH_3X. Experimentally, Gas-phase reactions of NH_2Cl with a series of nucleophiles including OH^- have been investigated using the selected ion flow tube technique by Bierbaum's group[23]. This experiment confirmed Gluknovtsev's *ab initio* study[22] that the S_N2 reaction at nitrogen is more facile than the corresponding reaction at carbon.

In solution phase, so far as we know, there have been experimental investigations of NH_2Cl with OH^- in alkaline solution[24,25] and NH_2Cl with OH radical in aqueous solution[26]; however, there have been no theoretical and experimental reports on the title reaction in aqueous solution. So here we apply the combined quantum mechanical and molecular mechanics (QM/MM) methodology[27,28] to study the $NH_2Cl + OH^-$ in aqueous solution, and to determine its accurate potential of mean force (PMF) at CCSD(T)/MM level of theory, solution effects on the PMF and to compare it with the corresponding S_N2 reaction at carbon.

In this study, we assume that only the solute atoms ($NH_2Cl + OH^-$) are involved in the bond breaking and bond forming process, therefore the solute part was treated using quantum mechanism method and the water solution was treated using the molecular mechanism method with an explicit water model[29,30]. Nonetheless, even under the QM/MM scheme, due to the huge computational cost on the system in

solution, one normally uses the *ab initio* Hartree-Fock (HF)[31] or DFT method[32,33] to treat the QM region. However, the benchmark work by Zhao and Truhlar[34-36] in gas phase shows that the DFT method usually underestimates the reaction barrier height when compared with the experiment result. So in order to get a more accurate description of the reaction pathway beyond the HF and DFT methods, we want to determine the reaction barrier height on the 'golden-standard' CCSD(T)[37, 38] method. However, direct CCSD(T) computational cost is too huge to be realistic for the whole dynamical calculation process; consequently, we use multi-levels of QM theory, ESP (effective electrostatic potential), DFT and CCSD(T), to treat the QM region during the different stages of our QM/MM calculation to eventually obtain the PMF on the accurate CCSD(T) method. Hence a multi-level QM/MM (ML-QM/MM) approach[29,30,39] is applied to study the $NH_2Cl + OH^-$ in aqueous solution. Such ML-QM/MM approach under the CCSD(T)/MM level has been proven to achieve more accurate reaction barrier heights for reactions in solution phase[40,41] than the usual DFT treatment to the QM part.

For the reasons discussed above, in this study, the ML-QM/MM approach was employed to study the $NH_2Cl + OH^-$ reaction mechanism in water: The first purpose of our study is to investigate this reaction mechanism in water and to calculate the accurate PMF for the title reaction at CCSD(T)/MM level of theory; the second purpose is to determine the solution effects to the reaction; the third purpose of our study is to compare our calculated reaction profile in water with the estimated one

using available gas-phase data; finally, we can compare our calculated rate constant with the S_N2 reaction at carbon in aqueous to determine their reactivities in solution.

Ⅱ. METHODOLODY

2.1. Multi-level QM/MM approach

As stated above, the whole reaction system was divided into two parts: the QM region which includes the solute $NH_2Cl + OH^-$ and the MM region which includes the aqueous solution. The MM water molecules were treated using an explicit SPC/E water model[42]. Thus the total energy of the whole reaction system can be written as:

$$E_{total} = E_{QM}(\boldsymbol{r};\psi) + E_{QM/MM}(\boldsymbol{r},\boldsymbol{R};\psi) + E_{MM}(\boldsymbol{R}) \quad (1)$$

Where $\boldsymbol{r}$, $\boldsymbol{R}$, and ψ represent the coordinates of the QM region, coordinates of the MM region and the ground state electronic wavefunction of the QM region respectively. $E_{QM}(\boldsymbol{r};\psi)$ is the energy of the QM region which has the gas phase expression and $E_{MM}(\boldsymbol{R})$ is the molecular mechanical energy of the MM part. The $E_{QM/MM}(\boldsymbol{r},\boldsymbol{R};\psi)$ represents the interactions between the QM part and the MM part :

$$E_{QM/MM} = E_{electrostatic} + E_{vdw} + E_{nuclear-nuclear} \quad (2)$$

The first term describes the electrostatic interactions, the second term is the van der Waals interactions and the third term is the nuclear solute-solvent interactions. The electrostatic interaction contribution can be simplified by introducing an effective classical representation for the solute-solvent interactions,

$$E_{electronstatic} = \sum_I \int \frac{Z_I \rho(\boldsymbol{r}')}{|\boldsymbol{R}_I - \boldsymbol{r}'|} d\boldsymbol{r}' = \sum_{i,I} \frac{Z_I Q_i}{|\boldsymbol{R}_I - \boldsymbol{r}_i|} = E_{ESP}(\boldsymbol{r},\boldsymbol{R},Q) \quad (3)$$

Where ρ represents the solute electron density, Z_I is the solvent classical charge. Here the QM electronic density is represented by effective electrostatic potential (ESP)

charges (Q_i), which is fitted from the *ab initio* calculation of the electrostatic potential surface of the QM region. The ESP representation forms the base-level theory for the QM region.

As mentioned above, we use the ML-QM/MM approach during different steps of calculation. First of all, we obtain the free energy difference between two adjacent points A and B along the PMF reaction pathway under the DFT/MM level of theory:

$$\Delta W_{AB}^{DFT} = (\Delta W_{AA}^{DFT\leftarrow ESP} + \Delta W_{BB}^{DFT\leftarrow ESP}) + \Delta W_{AB}^{ESP} \quad (4)$$

The term in brackets denotes free energy difference for changing the description from ESP to DFT level of theory at fixed solution A and B configurations. ΔW_{AB}^{ESP} gives the MM contribution to the PMF at the ESP/MM level from fixed A to B solute configurations. Secondly, based on the free energy of DFT/MM level of theory, the expected free energy difference at CCSD(T)/MM level can be calculated as

$$\Delta W_{AB}^{CC} = (\Delta W_{AA}^{CC\leftarrow DFT} + \Delta W_{BB}^{CC\leftarrow DFT}) + \Delta W_{AB}^{DFT} \quad (5)$$

Here CCSD(T)/MM PMF is the sum of PMF on DFT/MM level of theory and the free energy difference of shifting the free energy from DFT to CCSD(T) levels of theory.

In this study of the $NH_2Cl + OH^-$ in water solution, for the DFT method, we use both the M06-2X and B3LYP exchange-correlation functionals to determine the PMF, and to see how DFT results behave under these two functionals. Then we shift calculations from the DFT/M06-2X and DFT/B3LYP levels of theory to the CCSD(T) level of theory to compare the corresponding results. The aug-cc-pVDZ basis set is used for both the DFT and CCSD(T) methods.

2.2. Numerical simulation details

The reaction solute of $NH_2Cl…OH^-$ was solvated into a 34.4 Å cubic box including 1353 water molecules. These water molecules were treated as the MM region with an explicit SPC/E water model. A cutoff radius of 15 Å was used around the QM region to separate the interactions: within the cutoff radius, $NH_2Cl…OH^-$ interacts with the water atoms via bonded interactions, electrostatic interactions and Van der Waals interactions. The QM region electrons move in the potential generated by the nuclei in the QM system with charges Q_i, the charges of the MM atoms Z_I and the effective core potential of the boundary atoms. Outside the cutoff radius, the QM region only have Coulombic interactions between the MM charges and the QM ESP charges. The QM region was first treated using the DFT method with B3LYP and M06-2X functionals combined with the aug-cc-pvDZ basis set. The van der Waals parameters for QM region were taken from standard Amber force field[43]. The NWChem computational chemistry package[44] was used to determine the PMF in solution.

The first step of our calculations was to prepare an initial reactant complex. We took the $NH_2Cl…OH^-$ reactant complex from the gas phase reaction[19] and embedded it into the water box described above, then the whole system was optimized with a multi-region optimization. After the above step, we equilibrated the solvent water with 40ps molecular dynamics simulation with a time step of 0.001ps. During the equilibration, the fixed QM region was represented by the ESP charges calculated in the prior optimization step. Following the equilibration calculation, the whole system was optimized to generate the initial reactant complex of the title reaction in water solution.

The second step of our calculations was to find a product complex. Based on the obtained initial reactant complex in solution, a N-Cl bond breaking and N-O bond forming process was carried out to search and get the product state. Then the multi-region optimization and equilibration procedures, the same as for the reactant complex, were applied to get the initial product complex.

The third step of our calculation is to determine the transition state. Using the optimized initial reactant state and product state, the climbing image nudged elastic band (NEB) method[45], which is a modified version of the regular NEB, was applied to get the an initial reaction pathway. The reaction pathway was mapped out using ten images from the reactant to product state. The structure of the top image on the reaction pathway was isolated for a transition-state search. The obtained transition state was confirmed by a frequency calculation in water solution with one imaginary frequency.

The fourth step of our calculation is to obtain the final reactant and product complexes. The vibrational normal mode of the imaginary frequency was displaced toward the reactant and product sides respectively, and the multi-region optimization was performed on the displacements again to obtain the final reactant and product complexes.

The fifth step of our calculation is to get a converged reaction pathway. The final reaction pathway was mapped using the final reactant and product with 10 images, then the molecular dynamics simulation was performed for each image along the

reaction pathway for 40ps with a time step of 0.001ps. This step was repeated until the final NEB reaction pathway was converged.

Finally, the PMF was calculated from the converged 10 images along the reaction pathway. The PMF of the DFT/MM level was calculated first based on Eq. 4; then using the Hartree-Fock reference orbitals obtained under the DFT calculation, the CCSD(T) correlation energy under the CC level was calculated; finally, the sum of the Hartree-Fock and CC correlation energies gave the CCSD(T)/MM energy based on Eq. 5.

Ⅲ. RESULTS AND DISCUSSIONS

3.1. Stationary points on the reaction pathway

The optimized reactant structures in water solution under both the DFT/B3LYP and DFT/M06-2X approaches are shown in Figure 1(A). The two structures obtained using different exchange-correlation functionals only have very small differences between them. Similar to the reactant complex in gas phase[19], the O atom in the nucleophile forms a hydrogen bond with one of the hydrogens in the substrate; the hydrogen bond obtained using M06-2X functional is a little longer than the one using B3LYP by 0.02 Å. Nonetheless, the hydrogen bond in solution, about 1.70 Å, is much longer than that of 1.5 Å in gas phase[19]. This is understandable because charge screening on the OH^- by the surrounding water molecules reduces the interaction between the substrate and the nucleophile, which leads to the bond elongation.

The transition state structures in water are shown in Figure 1(B). They are verified by having a single imaginary frequency of 285i cm^{-1} with B3LYP and 299i cm^{-1} with

M06-2X. The transition state structures show that the hydroxide ion rotates away from facing the H atom in the reactant to face, and to approach the N center. In the mean time, the chlorine atom is leaving N atom. Therefore, this is a concerted, bond forming and bond breaking process, which shows a typical S_N2 back-side attack reaction mechanism. With the M06-2X functional, the N-Cl bond length is 2.01 Å and N-O bond length 2.22 Å. The N-O bonds in solution under both functionals, 2.28 Å and 2.22 Å is longer than that in gas phase, 2.16 Å. Small difference exists for the transition state structures between the B3LYP and M06-2X functionals.

Figure 1(C) shows the product geometries with the leaving group Cl atom detached from the center N atom. The Cl atom totally detached from the N center does not appear in solution here. The reason is that the caging effect of the water solution hinders the total separation of the leaving group and the substrate. The distances between the substrate and the leaving group in water are 2.91 Å and 2.86 Å with B3LYP and M06-2X functionals respectively.

3.2. Potential of mean force

The PMFs along the NEB reaction pathway under DFT and CCSD(T) levels of theory as well as the solvation free energy contribution described by ΔW_{AB}^{ESP} term (see Equation 4) with B3LYP and M06-2X functionals are shown in Fig. 2. The reactant free energy is used as reference energy point and only relative free energy is computed along the reaction pathway. The barrier heights exhibit a big difference under the DFT/MM with B3LYP and M06-2X functionals. The one calculated with DFT(B3LYP)/MM level has a barrier height at 21.8 kcal/mol, the other with

DFT(M06-2X)/MM level 27.4 kcal/mol. Nonetheless, the barrier heights under the CCSD(T)/MM level of theory (using Eq. 5) obtained based on the above two DFT/MM calculations are very close: the one based on the DFT(B3LYP)/MM level of theory is 22.4 kcal/mol, and the one based on DFT(M06-2X)/MM level 22.9 kcal/mol. Our previous studies of the S_N2 reactions[40,41] at carbon show that barrier heights under CCSD(T)/MM level of theory show very good agreements with the experimental values while the ones under DFT(B3LYP)/MM level of theories underestimate the experimental barrier-height. Therefore, the barrier heights obtained under the CCSD(T)(B3LYP)/MM, 22.4 kcal/mol, and CCSD(T)(M06-2X)/MM, 22.9 kcal/mol should be close to its true barrier height. Thus, here we take the average value on the above two CCSD(T)/MM results, 22.7 kcal/mol, as our predicted barrier height for this reaction in water solution.

The above results indicates, compared to the CCSD(T)/MM average value 22.7 kcal/mol, that the DFT/B3LYP approach (21.8 kcal/mol) underestimates the reaction barrier height and the DFT/M06-2X (27.4 kcal/mol) overestimates the reaction barrier height. This is similar to the situation in gas phase wherein the DFT/B3LYP method usually underestimates the reaction barrier height[34] and the DFT/M06-2X method overestimate the reaction barrier height[46]. Based on our previous results of S_N2 reactions[40,41] at carbon with the CCSD(T)/MM level of theory and the current CCSD(T)/MM barrier heights, we can say that one needs to employ the 'golden-standard' CCSD(T) level of theory to predict reliable and accurate reaction barrier heights for reactions in solution phase.

According to the *ab initio* molecular dynamics investigation on OH^- with NH_2Cl by Yu's group[21], the gas phase barrier height by MP2 is 11.4 kcal/mol and 10.4 kcal/mol by CCSD(T). We see that the energy barrier in water, 22.7 kcal/mol, is much higher than those in gas phase. This means that the water environment has a very significant contribution to activation barrier, which hinders the reactivity compared to the same reaction in gas phase. This significant contribution from the aqueous solution to the barrier is because the transition state is less stabilized than the reactant by solvation. Relative to the reactant, the transition state is bulkier than the reactant. As a result, the reactant is more strongly solvated than the transition state from gas phase to solution, leading to the higher barrier in solution.

The contributions of aqueous solution to the PMF are reflected from two aspects: solvation contribution and polarization effect. The solvation contribution has been plotted in Figure 2 under both the CCSD(T)(B3LYP)/MM and CCSD(T)(M06-2X)/MM levels of theory. The contribution to barrier height is 10.3 kcal/mol with B3LYP and 13.5 kcal/mol with M06-2X. The polarization effect is caused by solution's perturbation to the solute electronic structure. By comparing the internal energy which excluded the solvation contribution from water and the gas phase energy which is obtained by excluding the interaction between the QM part and MM part, we obtained the polarization effects under the two CCSD(T) levels in Figure 3. It shows that the polarization effect raised 8.6 kcal/mol for the reactant state, 11.6 kcal/mol for the transition state and 5.3 kcal/mol for the product state under the CCSD(T)(B3LYP)/MM level of theory; while they are 7.3 kcal/mol, 8.3 kcal/mol and

4.1 kcal/mol respectively under the CCSD(T)(M06-2X)/MM level of theory. Consequently, the polarization effect under CCSD(T)(B3LYP)/MM level of theory raised the net barrier height by 3.0 kcal/mol, while 1.0 kcal/mol to the barrier height under the CCSD(T)(M06-2X)/MM level of theory. Therefore, for the total solution contribution to reaction barrier height, the solvation effect plays a major role in reducing the reactivity for this reaction in solution, which contributes about 46% and 59% to the reaction barrier height respectively under the CCSD(T)(B3LYP)/MM and CCSD(T)(M06-2X)/MM levels of theory. In total, the water solution contributes 13.3 kcal/mol to the reaction barrier height under the CCSD(T)(B3LYP)/MM level of theory, which is close to the contribution under the CCSD(T)(M06-2X)/MM level, 14.6 kcal/mol.

3.3. Comparison of reaction profiles

In Figure 4, we compared our calculated reaction profiles in solution under both CCSD(T)(B3LYP)/MM and the CCSD(T)(M06-2X)/MM levels of theory with the estimated reaction profile. The estimated reaction profile was obtained by using the data from the gas-phase CCSD(T) level profile[21] and the solvation energies of the reactants and products from different theoretical studies: NH_2Cl (-5.3 kcal/mol)[47], OH^- (-106.4 kcal/mol)[48], NH_2OH (-14.48 kcal/mol)[49] and Cl^- (-73.89 kcal/mol)[50] respectively. The above data produces a free reaction energy in aqueous solution with -21.4 kcal/mol which has an excellent agreement with the one -21.7 kcal/mol from our CCSD(T)(M06-2X)/MM calculation, and also agree with the one -26.0 kcal/mol from the CCSD(T)(B3LYP)/MM calculation. From this comparison, it shows that,

overall, the CCSD(T)(M06-2X)/MM gives a better reaction pathway profile than the CCSD(T)(B3LYP)/MM does.

3.4. Comparison of S_N2 reaction at nitrogen and at carbon

In gas phase studies, the experimental measurement by Bierbaum et al.[23] found that the rate of NH_2Cl with OH^- is about 3.33×10^{-9} $cm^3mole^{-1}s^{-1}$, while the corresponding S_N2 reaction rate of CH_3Cl with OH^- by DePuy et. al[51] is about 2.0×10^{-9} $cm^3mole^{-1}s^{-1}$, which means that the S_N2 reaction at nitrogen has a faster reactivity than that at carbon in gas phase. So for the current reaction at nitrogen in aqueous solution, we also want to compare its reactivity with the corresponding reaction at carbon in aqueous solution.

We used the thermodynamics equation[52,53] of the transition state theory to calculate the reaction rates in solution,

$$k = A\,exp(-\frac{\Delta W_a^+}{RT}) \qquad (6)$$

where A is defined as $(k_BT/h)\cdot(RT/P)$, and k_B, h, R, P and ΔW_a^+ denote the Boltzmann constant, Plank constant, gas phase constant, standard state pressure and activation free energy, respectively. Our calculation found that the barrier height for the current reaction at nitrogen is predicted at 22.7 kcal/mol, so based on the above equation, a rate constant of 5.67×10^{-24} $cm^3molecule^{-1}s^{-1}$ at 298K is obtained. The experimental barrier height[14] for the $CH_3Cl + OH^-$ in water, 24.3 kcal/mol, is about 1.6 kcal/mol larger than that of the above reaction at nitrogen; the measured rate is 1.01×10^{-26} $cm^3molecule^{-1}s^{-1}$, which is about two orders of magnitude larger than the rate of the above reaction at nitrogen. Therefore, in aqueous solution, the S_N2

reaction at nitrogen still is a faster reaction than the corresponding S_N2 reaction at carbon.

Ⅳ. CONCLUSION

Using the ML-QM/MM methodology, the S_N2 reaction of $NH_2Cl + OH^-$ in water solution was studied. We identified the geometries of reactant, product and transition states, obtained reaction free energy profiles, and determined the contribution from the solution effects to the potential of mean force. The two activation barriers were much different under the DFT/MM level of theory, 21.8 kcal/mol with the B3LYP and 27.4 kcal/mol with the M06-2X exchange-correlation functionals, respectively. However, when shifted from the DFT level of theory with the two functionals to the CCSD(T) level of theory, the CCSD(T)(B3LYP)/MM and CCST(T)(M06-2X)/MM produced very close results with the barrier heights at 22.4 kcal/mol and 22.9 kcal/mol respectively. Comparing the CCSD(T)/MM reaction profile with the estimated profile obtained using gas phase data, we found that, the free reaction energy from our CCSD(T)(M06-2X)/MM calculation has an excellent agreement with the one obtained using available gas-phase data.

The water solution significantly reshapes the reaction profile: it contributes ~13.3 kcal/mol to the reaction barrier height under the CCSD(T)(B3LYP)/MM level of theory, and 14.6 kcal/mol under the CCSD(T)(M06-2X)/MM level of theory. Among the two solution effects, solvation effect and polarization effect, the solvation effect plays a major role in reducing the reactivity for this reaction in solution.

Our predicted reaction barrier is 22.7 kcal/mol for this N center S_N2 reaction in aqueous solution. The calculated rate constant is 5.67×10^{-24} $cm^3molecule^{-1}s^{-1}$ at 298K, which is about two orders of magnitude larger than that of the corresponding reaction at carbon in aqueous solution. Therefore, for these two S_N2 reactions in solution, the S_N2 reaction at nitrogen has a bigger reactivity than the S_N2 reaction at carbon.

ACKNOWLEDGMENTS

D.Y. Wang thanks the National Natural Science Foundation of China (Grant No. 11074150) and Taishan Scholarship fund for supporting this work. The computation work was carried out at the Shenzhen Supercomputer Center of China.

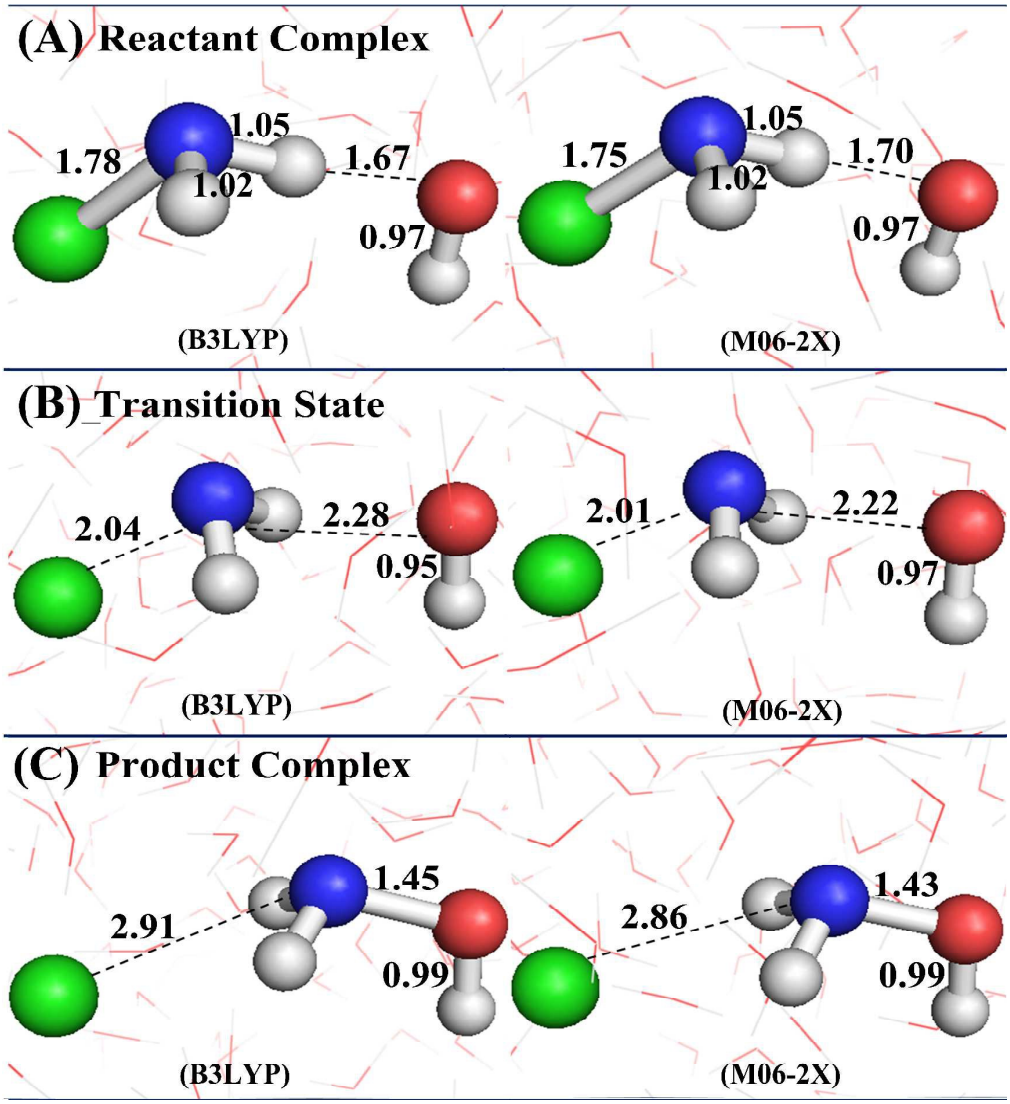

Figure 1. Structures of the reactant complex (A), transition state (B), and product complex (C) for the reaction, $NH_2Cl + OH^- \rightarrow NH_2OH + Cl^-$ in aqueous solution with both the DFT(B3LYP)/MM and DFT(M06-2X)/MM levels of theory. The units of the data in figure are angstroms.

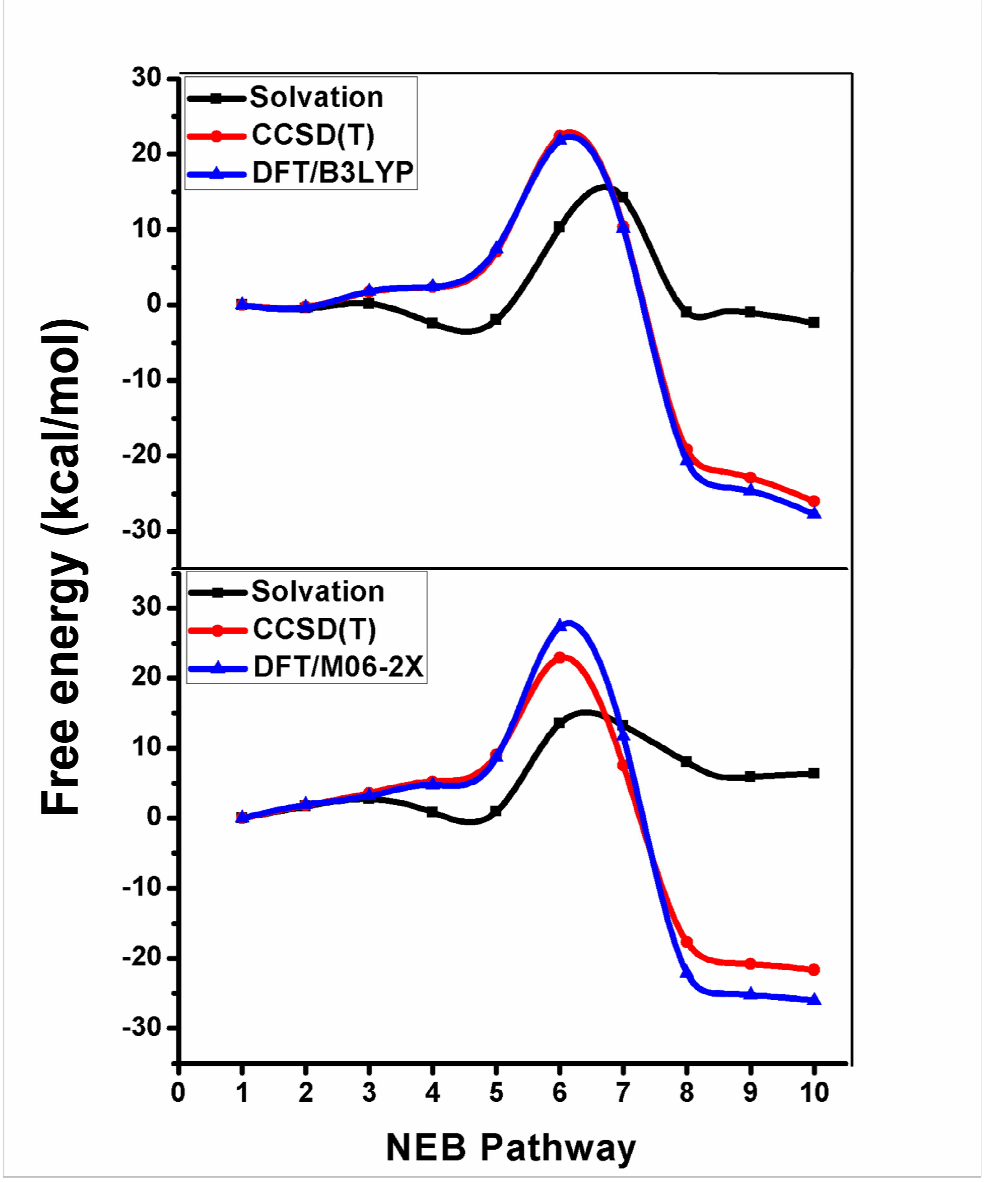

Figure 2. Comparison of potentials of mean force calculated at the DFT/MM and CCSD(T)/MM levels of theory and solvation contribution using the reactant state as a reference point.

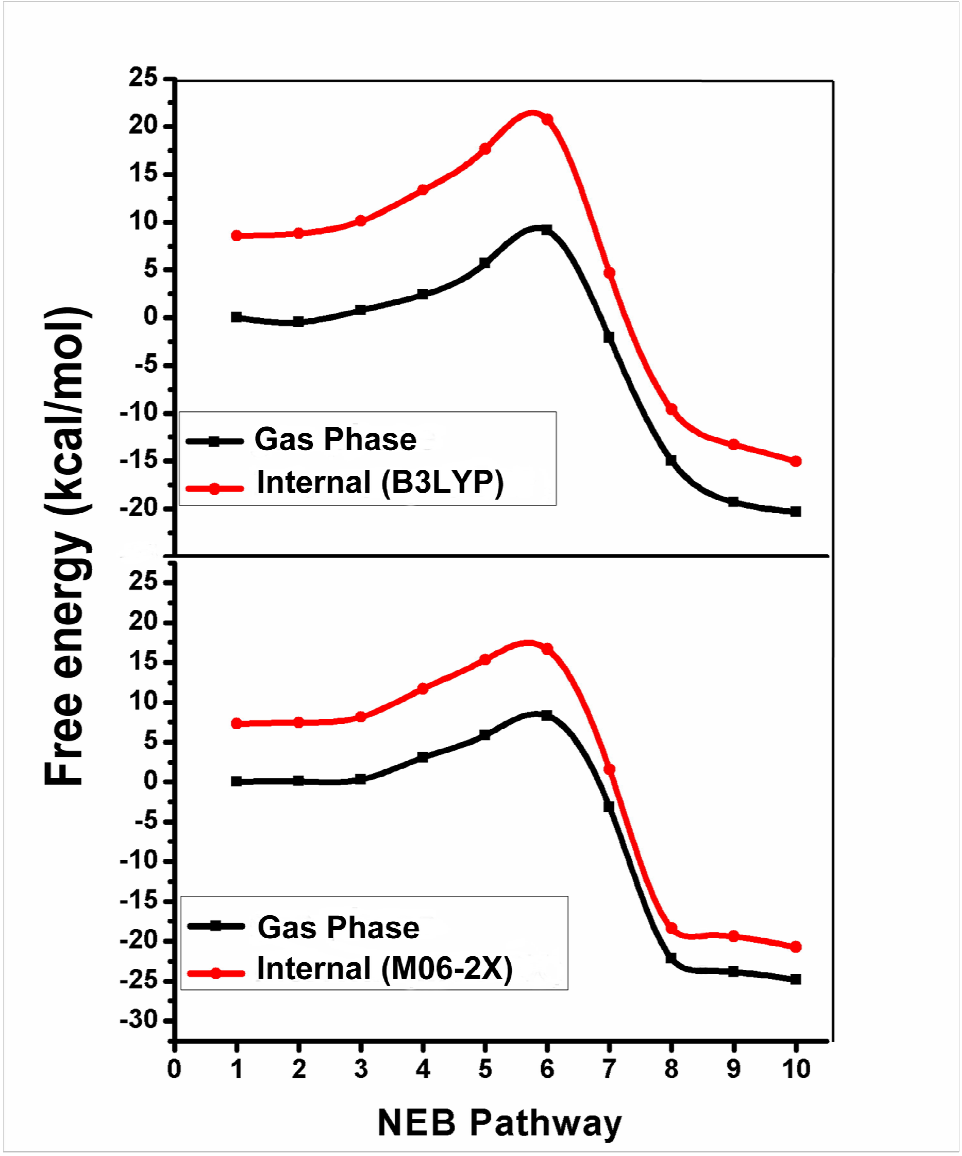

Figure 3. Comparison between gas-phase and the internal energies along the NEB pathway at the CCSD(T)/MM level of theory using the gas-phase energy of the reactant as a reference point.

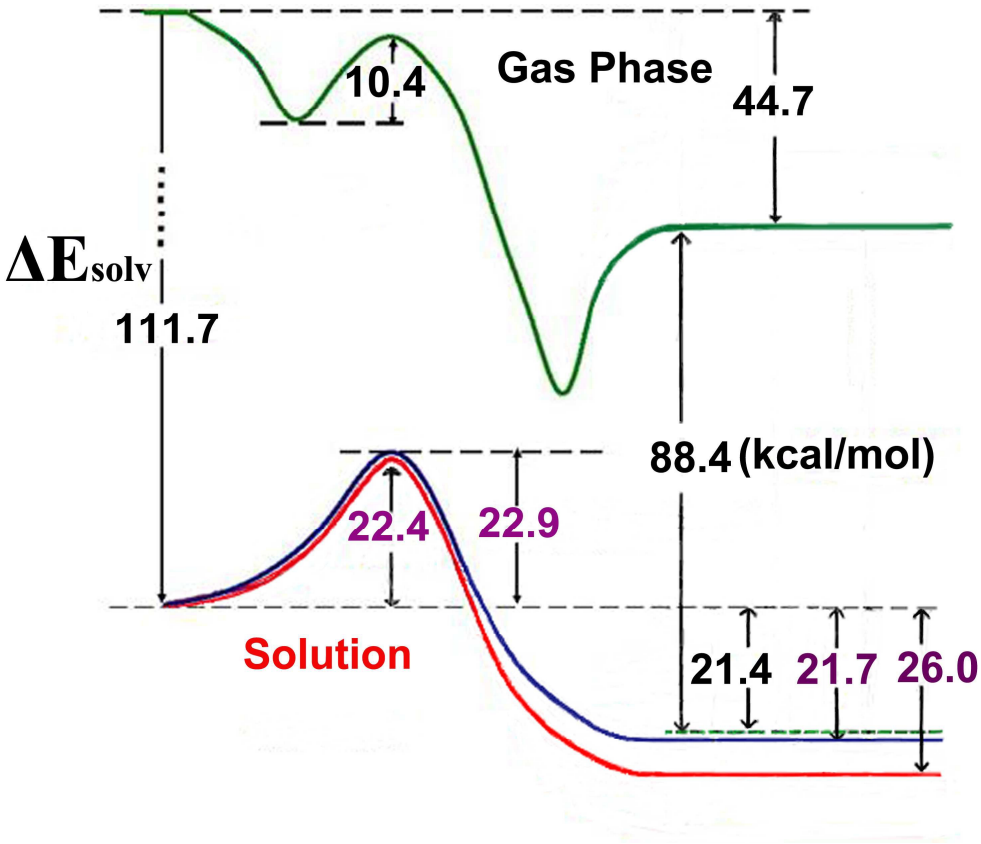

Figure 4. Ccomparison between the estimated reaction profile in solution (the green line) and our calculated reaction profiles under the CCSD(T)(B3LPY)/MM level of theory(red line) and CCSD(T)(M06-2X)/MM(blue line) level of theory.

References

(1) C. K. Ingold, Cornell University Press: Ithaca, New York, 1953.

(2) S. S. Shaik, H. B. Schlegel and S. Wolfe, Wiley, New York , 1992.

(3) W. L. Hase, Science, 1994, **266**, 998.

(4) J. K. Hwang, G. King, S. Creighton and A. Warshel, J. Am. Chem. Soc., 1988, **110**, 5297.

(5) M. N. Glukhovtsev, A. Pross and L. Radom, J. Am. Chem. Soc., 1996, **118**, 6273.

(6) S. Parthiban, G. de Oliveira and J. M. L. Martin, J. Phys. Chem. A, 2001, **105**(5), 895.

(7) J. K. Laerdahl and E. Uggerud, Int. J. Mass Spectrom., 2002, **214**, 277.

(8) S. Schmatz, ChemPhysChem, 2004, **5**, 600.

(9) R. Otto, J. Brox, S. Trippel, M. Stei, T. Best and R. Wester, Nat. Chem., 2012, **4**, 534.

(10) I. Szabó and G. Czakó, Nat.Commun., 2015, **6**, 5972.

(11) I. Szabó and G. Czakó, J. Phys. Chem. A, 2015, **119**, 3134.

(12) R. H. Bathgate and E. A. Moelwyn-Hughes, J. Chem. Soc., 1959, **439**, 2642.

(13) P. M. Hierl, J. F. Paulson and M. J. Henchman, J. Phys. Chem., 1995, **99**(42), 15655.

(14) B. D. Wladkowski and J. I. Brauman, J. Phys. Chem., 1993, **97**, 13158.

(15) J. Xie, R. Otto, J. Mikosch, J. Zhang, R. Wester and W. L. Hase, Acc. Chem. Res. 2014, **47**, 2960.

(16) M. Stei, E. Carrascosa, M. A. Kainz, A. H. Kelkar, J. Meyer, I. Szabó, G. Czakó and R. Wester, Nat. Chem., 2015.

(17) U.S. Environmental Protection Agency, Toxic and Priority Pollutants Under the Clean Water Act, 2014. http://water.epa.gov/scitech/methods/cwa/pollutants.cfm

(18) Centers for Disease Control and Prevention, Disinfection with Chloramine, 2015. http://www.cdc.gov/healthywater/drinking/public/chloramine-disinfection.html

(19) M. Bühl and H. F. Schaefer, J. Am. Chem. Soc., 1993, **115**, 9143.

(20) Y. M. Xing, X. F. Xu, Z. S. Cai, X. Z. Zhao and J. P. Cheng, Chem. Phys., 2004, **298**, 125.

(21) F. Yu, L. Song and X. G. Zhou, Comput. Theor. Chem., 2011, **977**, 86.

(22) M. N. Glukhovtsev, A. Pross and L. Radom, J. Am. Chem. Soc., 1995, **117**, 9012.

(23) R. Gareyev, S. Kato and V. M. Bierbaum, J. Am. Soc. Mass Spectrom., 2001, **12**, 139.

(24) M. Anbar and G. Yagil, J. Am. Chem. Soc., 1962, **84**, 1790.

(25) W. J. Le Moble, Tetrahedron Lett., 1966, **7**, 727.

(26) H. D. Johnson, W. J. Cooper, S. P. Mezyk and D. M. Bartels, Radiat. Phys. Chem., 2002, **65**, 317.

(27) A. Warshel and M. Levitt, J. Mol. Biol., 1976, **103**, 227.

(28) A. Warshel, Annu. Rev. Biophys. Biomol. Struct., 2003, **32**, 425.

(29) H. Y. Yin, D. Y. Wang and M. Valiev, J. Phys. Chem. A, 2011, **115**, 12047.

(30) T. T. Wang, H. Y. Yin, D. Y. Wang and M. Valiev, J. Phys. Chem. A, 2012, **116**, 2371.

(31) C. F. Fischer, (Wiley, New York, 1977).

(32) P. Hohenberg and W. Kohn, Phys. Rev., 1964, **136**, B864.

(33) W. Kohn and L. J. Sham, Phys. Rev., 1965, **140**, A1133.

(34) Y. Zhao, N. González-García and D. G. Truhlar, J. Phys. Chem. A, 2005, **109**, 2012.

(35) Y. Zhao and D. G. Truhlar, Acc. Chem. Res., 2008, **41**, 157.

(36) J. J. Zheng, Y. Zhao and D. G. Truhlar, J. Chem. Theory Comput., 2009, **5**, 808.

(37) J. F. Stanton and R. J. Bartlett, J. Chem. Phys., 1993, **98**, 7029.

(38) R. J. Bartlett and M. Musiał, Rev. Mod. Phys., 2007, **79**, 291.

(39) M. Valiev, B. C. Garrett, M. K. Tsai, K. Kowalski, S. M. Kathmann, G. K. Schenter and M. Dupuis, J. Chem. Phys., 2007, **127**, 051102.

(40) Y. L. Xu, T. T. Wang and D. Y. Wang, J. Chem. Phys., 2012, **137**, 184501.

(41) Y. L. Xu, J. X. Zhang and D. Y. Wang, Phys. Chem. Chem. Phys., 2014, **16**, 19993.

(42) H. J. C. Berendsen, J. R. Grigera and T. P. Straatsma, J. Phys. Chem., 1987, **91**, 6269.

(43) T. Fox and P. A. Kollman, J. Phys. Chem. B, 1998, **102**, 8070.

(44) M. Valiev, E. J. Bylaska, N. Govind, K. Kowalski, T. P. Straatsma, H. J. J. Van Dam, D. Wang, J. Nieplocha, E. Apra, T. L. Windus and W. A. de Jong, Comput. Phys. Commun., 2010, **181**, 1477.

(45) G. Henkelman, B. P. Uberuaga and H. Jónsson, J. Chem. Phys., 2000, **113**, 9901.

(46) F. Cozzi, R. Annunziata, M. Benaglia, K. K. Baldridge, G. Aguirre, J. Estrada, Y. Sritana-Anant and J. S. Siegel, Phys. Chem. Chem. Phys., 2008, **10**, 2686.

(47) Y. D. Liu, M. Selbes, C. Zeng, R. Zhong and T. Karanfil, Environ. Sci. Technol., 2014, **48**, 8653.

(48) M. W. Palascak and G. C. Shields, J. Phys. Chem. A, 2004, **108**, 3692.

(49) M. I. Fernández, M. Canle, M. V. García and J. A. Santaballa, Chem. Phys. Lett., 2010, **490**, 159.

(50) E. J. Bylaska, D. A. Dixon, A. R. Felmy and P. G. Tratnyek, J. Phys. Chem. A, 2002, **106**, 11581.

(51) C. H. DePuy, S. Gronert, A. Mullin and V. M. Bierbaum, J. Am. Chem. Soc., 1990, **112**, 8650.

(52) R. Daudel, G. Leroy, D. Peeters and M. Sana, *Quantum Chemistry* (John Wiley and Sons, Chichester, U.K, 1983).

(53) Y. Okuno, Chem. Eur. J., 1997, **3**, 212.

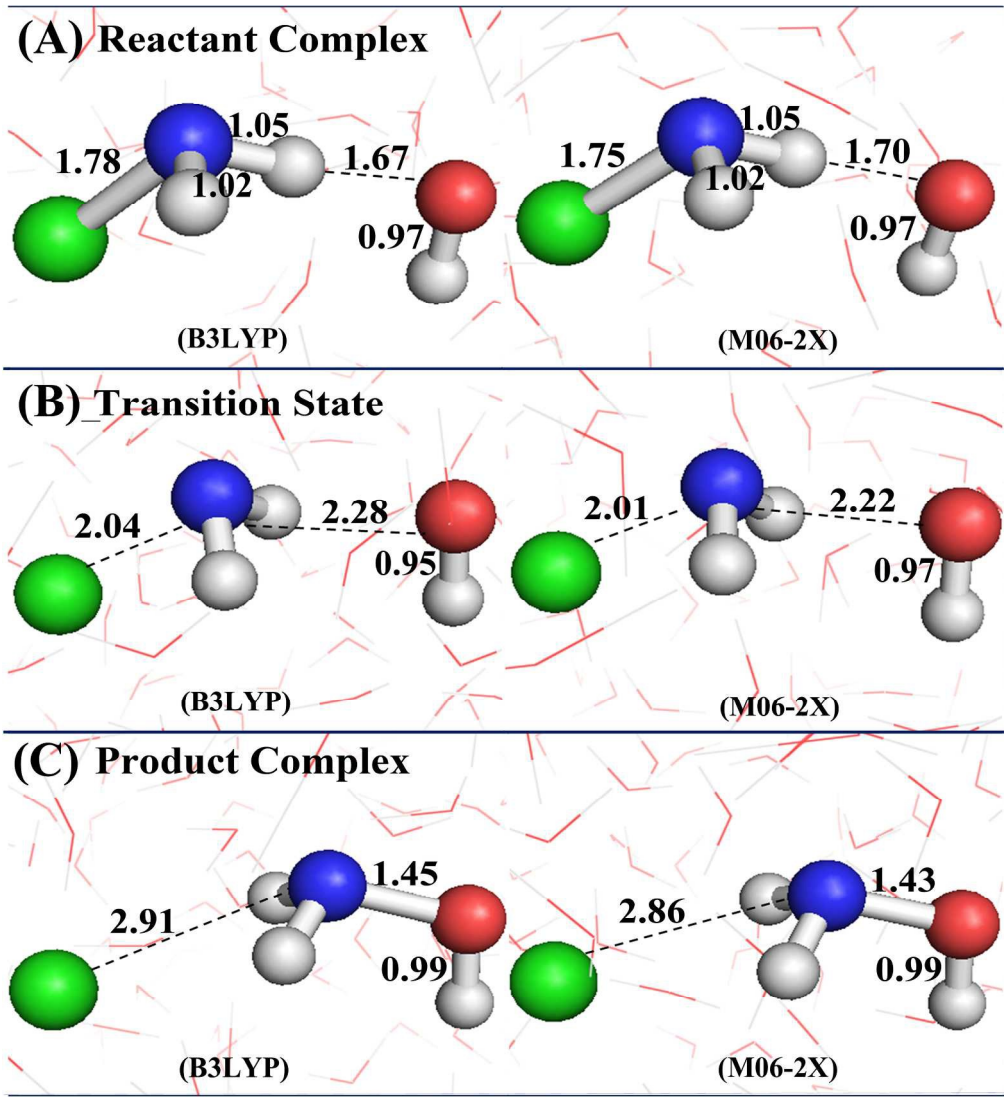

109x119mm (600 x 600 DPI)

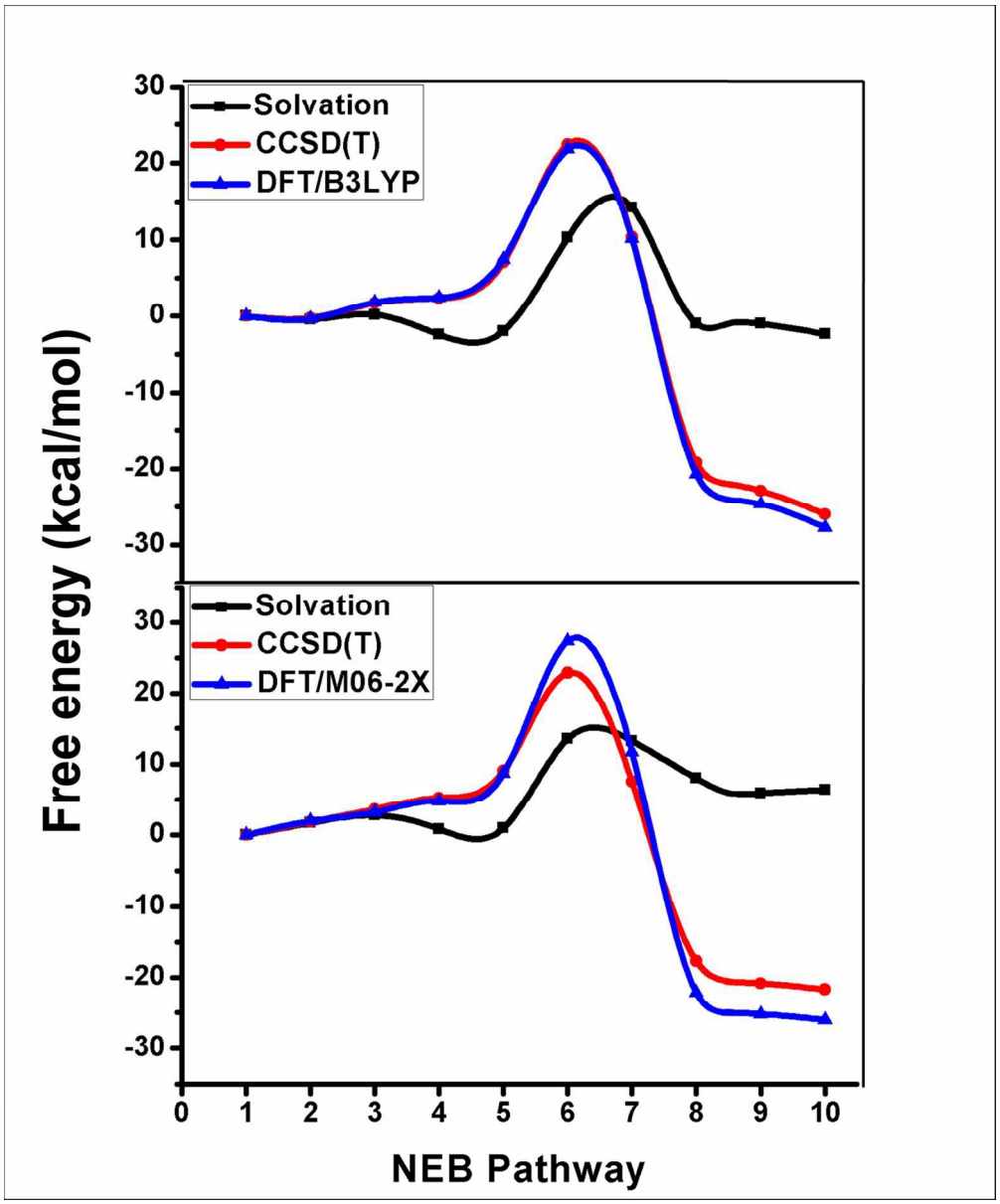

80x96mm (600 x 600 DPI)

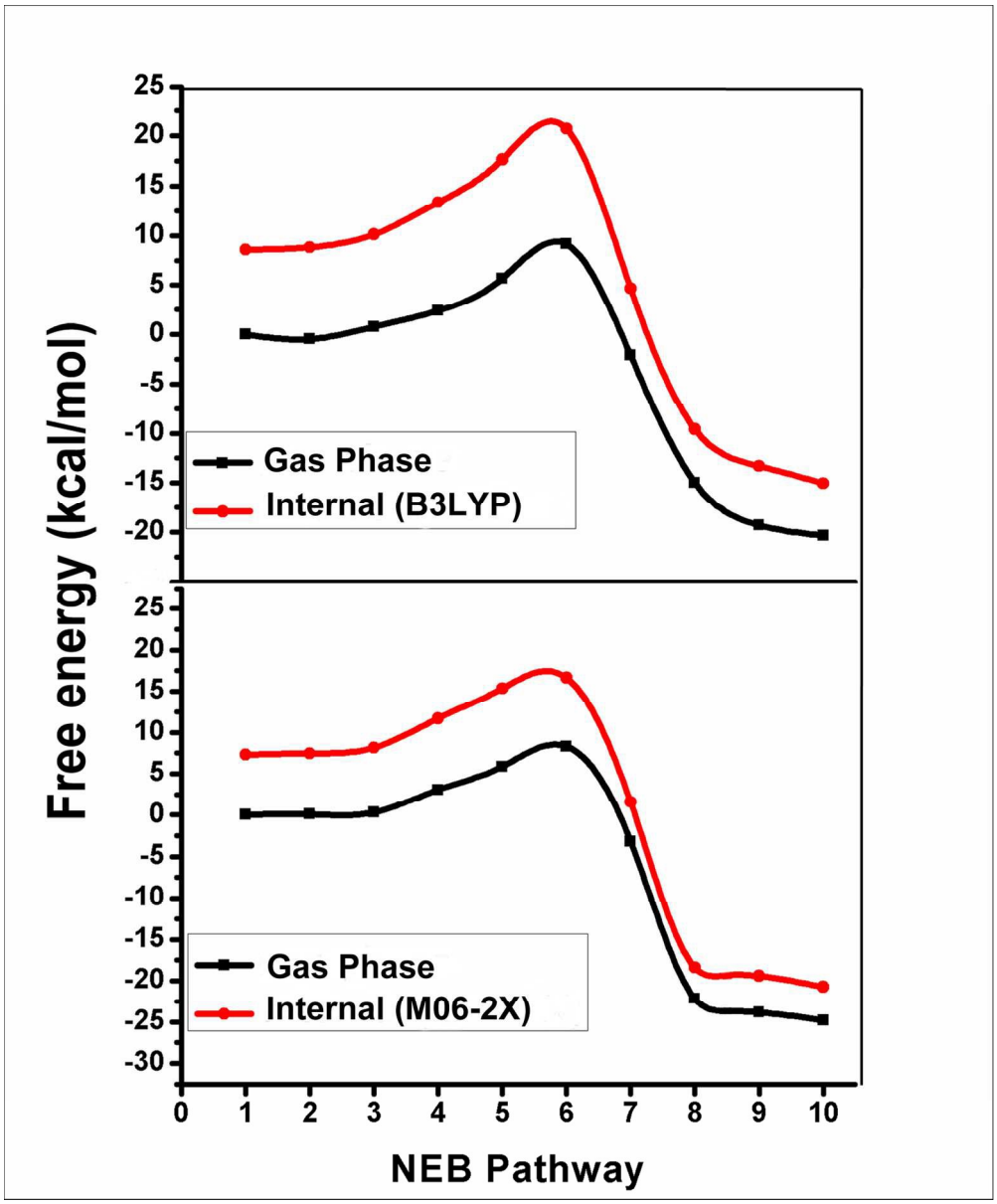

80x96mm (600 x 600 DPI)

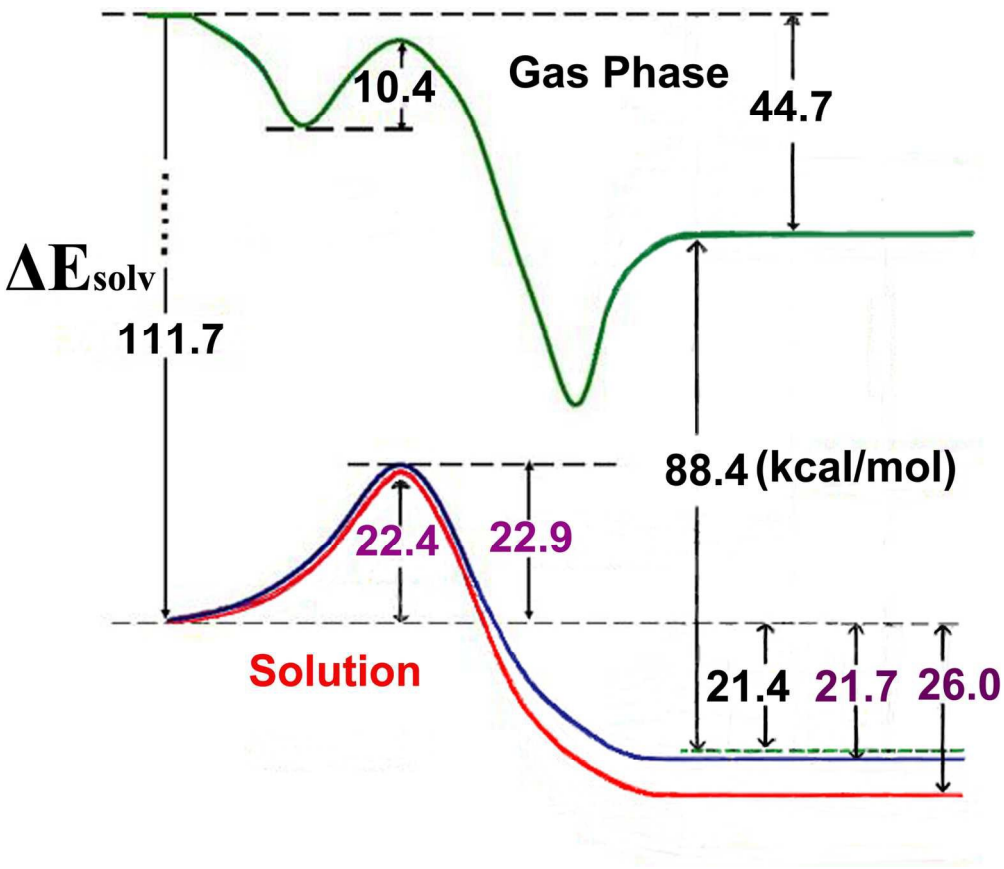

80x68mm (600 x 600 DPI)